ACS Energy LETTERS

http://pubs.acs.org/journal/aelccp

3D Printing Enabled Highly Scalable Tubular Protonic Ceramic Fuel Cells

Minda Zou, Jacob Conrad, Bridget Sheridan, Jiawei Zhang,* Hua Huang, Shenglong Mu, Tianyi Zhou, Zeyu Zhao, Kyle S. Brinkman, Hai Xiao, Fei Peng, and Jianhua Tong*

Cite This: *ACS Energy Lett.* 2023, 8, 3545−3551

Read Online

ACCESS | Metrics & More | Article Recommendations | Supporting Information

ABSTRACT: Protonic ceramic fuel cells (PCFCs) are clean and efficient power generation devices operating at intermediate temperatures. However, manufacturing difficulties have limited their commercialization, especially for promising tubular PCFCs. Herein, we report a cost-effective 3D printing technique for manufacturing large-area tubular PCFCs (e.g., 15.7 cm^2), featured with the use of commercial raw materials, a small amount of binder, and a CO_2 laser for rapid in situ drying. The technical advantages enable low-cost material preparation and efficient achievement of exemplary shape/dimension-controlled uniform microstructures in porous anode support, dense electrolyte, and porous cathode. The 3D-printed tubular PCFC (~12.5 cm^2) exhibits a power output of 2.45 W at 650 °C. Meanwhile, the long-term stability is confirmed during 200 h of operation. This novel 3D printing offers great potential to advance PCFCs from the laboratory to larger scales for realistic applications.

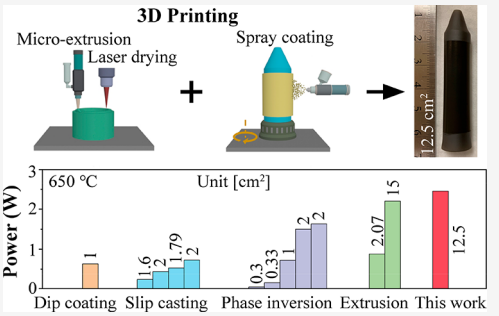

To build a low-carbon modern society, it is imperative to develop renewable energy devices that directly utilize clean and sustainable energy sources rather than pollution-intensive fossil fuels, such as coal and petroleum. Over the past decade, protonic ceramic fuel cells (PCFCs) have been leading energy devices in light of their high efficiency and low emissions for direct conversion of various renewable fuels, including H_2, hydrocarbons, ammonia, and alcohols, into electric power at intermediate temperatures (400 to 700 °C).[1,2] To date, impressive progress has been achieved in discovering novel component materials, tuning their microstructure, and building mathematical models to improve or analyze electrochemical performance and durability.[3,4] Nevertheless, these achievements are substantially limited to the laboratory scale and have not been broadly commercialized.

Generally, the typical geometries of PCFCs can be divided into two categories: planar and tubular types. The planar type is popular in laboratory tests due to the advantages of cheap manufacturing, simple structure, and easy integration. However, several prevailing challenges limit the scaleup and stacking of planar PCFCs, such as poor thermal stress tolerance,[5,6] unsatisfactory brittleness, and sealing issues.[7,8] Alternatively, tubular PCFCs are appealing candidates with great potential for commercialization. First, tubular geometry can help diminish thermal−chemical expansion effects and the rising stress concentration. Therefore, fast startup/shutdown and better thermal cycling stability can be realized.[9] Second, the high-temperature sealing issue can be mitigated by putting the sealing parts outside the high-temperature heating region.[10,11] Third, tubular geometry can offer greater mechanical strength than planar geometry with the same thickness so that portable characteristics and higher volumetric power densities can be achieved.[12,13] So far, several techniques have been utilized for manufacturing tubular supports of PCFCs, such as extrusion,[9,14−17] dip coating,[18−20] slip casting,[11,21−23] and phase inversion.[24−29]

Nonetheless, these techniques encounter a dilemma in scaling up with desirable microstructures and decent electrochemical performances and durability for PCFCs' applications. For example, the extrusion method can only produce simple symmetric geometries, and there is a shape-retaining issue during the drying process, bringing about reduced dimensional uniformity.[30] The dip coating technique needs to be improved with the problems of inconsistent coating thickness and erratic edge coverage. To utilize slip casting, uniquely designed and fabricated molds are needed, which increase the cost. Meanwhile, phase inversion process manufactured tubes usually have poor mechanical strength because of the highly

Received: July 5, 2023
Accepted: July 25, 2023
Published: July 28, 2023

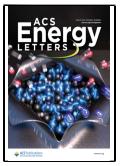

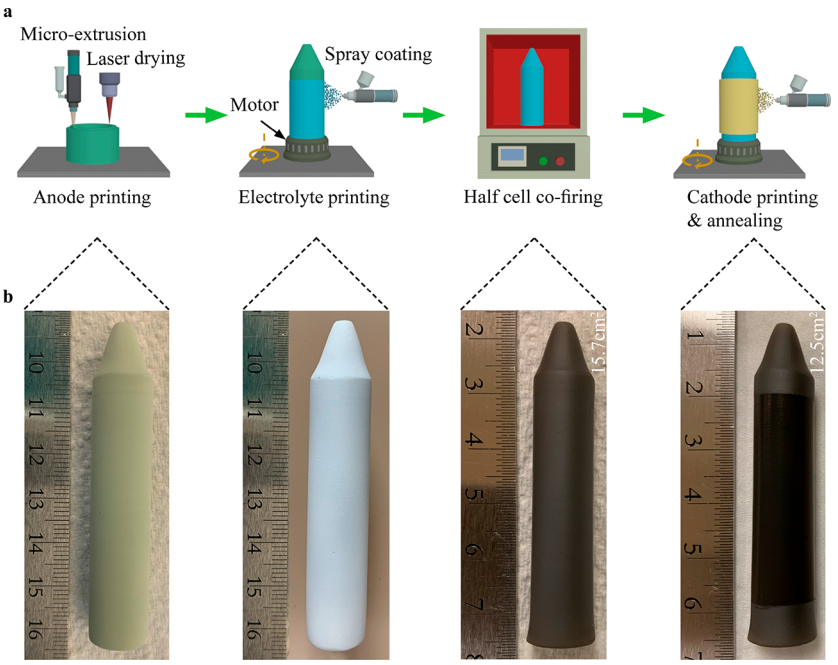

Figure 1. Schematic illustration of the manufacturing of a single tubular PCFC by 3DP. (a) Schematic of the manufacturing process. (b) Photographs of the tubular PCFC at different manufacturing steps.

anisotropic structure, tending to result in cell failure during their operation.[9] Hence, more applicable techniques capable of precise, reproducible, and customized manufacturing for large multilayered tubular cell structures are urgently required to be developed for PCFCs.

Additive manufacturing, also termed 3D printing (3DP), is a promising technique that offers significant opportunities in fabricating solid oxide fuel cells (SOFCs) due to the advantages of robotization, flexible customization, high accuracy, and high reproducibility. In the past decade, great efforts have been devoted to manufacturing the components of planar oxygen-ion conducting solid oxide fuel cells (O-SOFCs) via 3DP, such as inkjet printing,[31−33] aerosol jet printing,[34,35] digital light processing−stereolithography,[36−39] binder jetting,[40] and fused filament fabrication.[41] Recently, Huang et al.[42] reported 3D-printed microtubular O-SOFCs with high performance and excellent long-term durability. However, the method still needs an extra tubular mold with specific dimensions for tubular support printing. To the best of our knowledge, there is still a lack of reports on the 3D printing of tubular PCFC.

Herein, we reported manufacturing highly scalable single tubular PCFCs with an area as high as 15.7 cm^2 via a novel 3DP technique. The success relied on integrating digital microextrusion- and digital spray-coating-based additive manufacturing with laser drying. Notably, the produced single tubular cell exhibited excellent electrochemical performance (2.45 W at 650 °C, with an effective area of 12.5 cm^2) and promising long-term stability (a degradation rate of 0.00039 V h^{-1} during 200 h of operation). Our work suggests that 3DP could pave the way for the real-world applications of tubular PCFCs.

Figure 1 represents the manufacturing process of a complete tubular PCFC via 3DP. An entire single cell, including tubular anode support, electrolyte thin film, and cathode thin film, was successively printed via digital microextrusion and spray coating in our 3D printer. First, the anode paste, prepared by mixing the anode precursor powder, dispersant, deionized water, and binder, was fed to the microextruder through a plastic syringe. Second, the microextruder printed the anode paste on the printing platform with precise moving speed, dispensing, and trajectory following the sliced patterns from imported tubular 3D models on our house-made software. Microextrusion was used to print the tubular anode support because it can efficiently build bulk support, and offer far higher printing productivity than inkjet printing[31−33] and aerosol jet printing[34,35] techniques. Notably, we directly used commercial raw materials (i.e., metal oxides, carbonates, and organics) to prepare the paste. It can effectively reduce manufacturing costs compared to other 3D printing techniques. In comparison, inkjet printing and aerosol jet printing require ultrafine powders (submicrometer size) and low solid contents to prepare printable low-viscosity inks, leading to an increased cost; digital light processing−stereolithography needs expensive and special photosensitive resin in the slurry as well as lengthy debinding (hours to days).[36−39] Furthermore, during the conventional methods (extrusion, dip coating, and phase inversion) and fused filament fabrication, a high amount of binder (e.g., mass ratios of binder/ceramics are 10−25 wt %) is usually required, which may cause severe deformation issues during the postdrying/sintering processes.[18,27,29,30,41] In our case, the binder content (e.g., hydroxypropyl methylcellulose) in the paste is only 0.31 wt %, ensuring the feasible viscosity for printing and mitigating the deformation issues. Moreover, to further achieve good shape retainability of the anode and ensure good adhesion between printed layers without requiring high paste viscosity, a CO_2 laser was used for rapid in situ drying of the printed green body after printing each layer of the anode support. As such, we can achieve higher printing accuracy, especially when compared with binder jet printing,[40] which tends to have poor accuracies and surface finishes. Third, after obtaining the tubular anode support via alternating printing and laser drying processes, spray coating was used for printing the thin

https://doi.org/10.1021/acsenergylett.3c01345
ACS Energy Lett. 2023, 8, 3545−3551

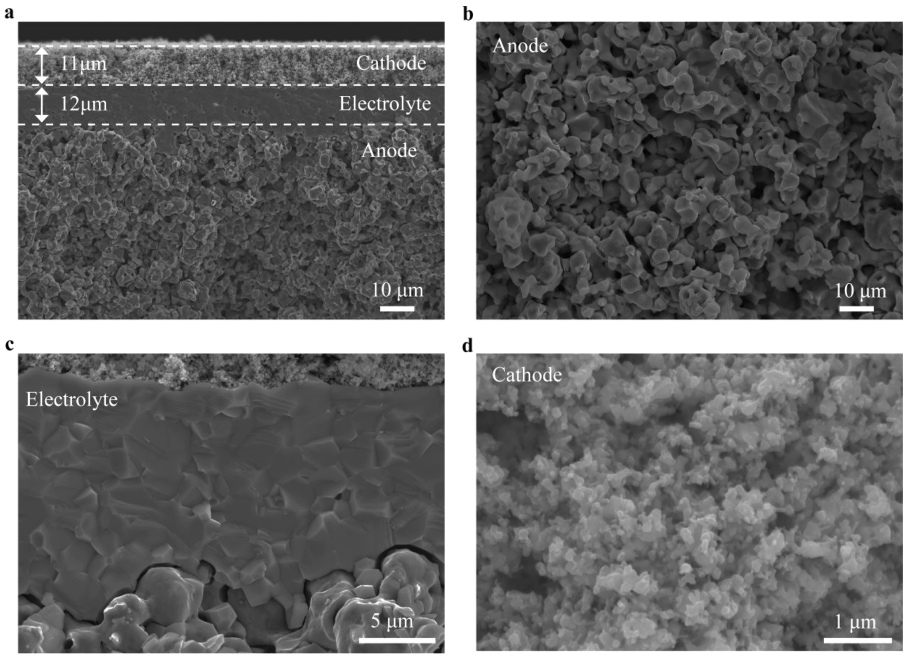

Figure 2. Microstructure of the large-scale tubular PCFC with a 12.5 cm^2 effective area after testing. (a) Cross-sectional SEM image of anode support (BCZY27−Ni)|electrolyte (BCZY27)|cathode (BCFZY0.1) sandwich structure. Enlarged cross-sectional SEM images of (b) the anode, (c) electrolyte/electrode interfaces, and (d) cathode.

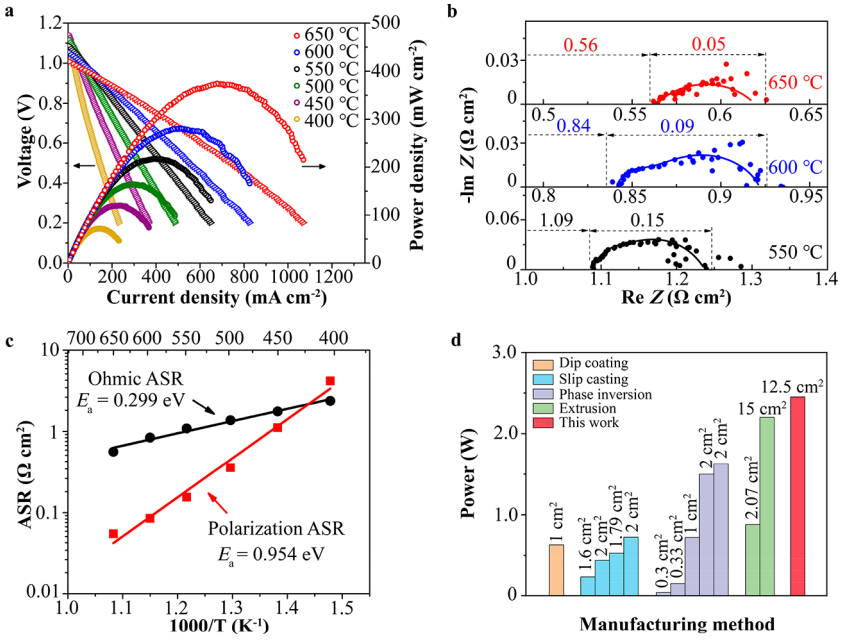

Figure 3. Electrochemical performance of a manufactured tubular PCFC. (a) *I*−*V* and *I*−*P* curves of a single PCFC tested at different temperatures. (b) EIS spectra for the single PCFC under OCV conditions at 550−650 °C. (c) Ohmic and polarization ASRs at 400−650 °C. (d) Power output of single tubular PCFCs fabricated via different methods at 650 °C.

electrolyte, which allows for accurate control of the thickness in the micrometer scale. Again, we still used pristine materials with no specific phase-formation process. The tube was rotated on a motor during the spray coating to ensure a homogeneous and efficient coating of the large-area thin films. Subsequently, the obtained half-cells were cofired through a cost-effective solid-state reactive sintering[1] method without prefiring the green anode to provide adequate mechanical strength for the following processing. Finally, the cathode thin green film was printed with a spray coating process similar to that of the electrolyte, followed by annealing in an external furnace to obtain single cells.

Figure 1b shows a large-scale uniform green anode tube with a cone-shaped end possessing an outer diameter of ∼13.5 mm and a height of ∼7.3 cm. After sintering, the half-cell retained the uniform tubular geometry, and the diameter decreased by ∼18.5% to ∼11 mm. The completed tubular PCFC has a uniform cathode thin film with a large effective area of ∼12.5 cm^2. The results indicate that the common dimensional errors observed in conventional extrusion methods from deformation

https://doi.org/10.1021/acsenergylett.3c01345
ACS Energy Lett. 2023, 8, 3545−3551

or cracks during processing can be readily avoided in the 3DP technique. In addition, precise control and reproducibility of electrolyte thickness were demonstrated with eight half-cells as shown in Figures S3 and S4, respectively. These advantages of our 3DP approach could enable the cost-effective manufacturing of scalable tubular PCFCs with precise and flexible geometry control.

Figure 2 shows the cross-sectional microstructure of the large-scale tubular PCFC with a 12.5 cm^2 effective area after testing. In Figure 2a, the cell has an anode support|electrolyte| cathode sandwich structure, where the anode, electrolyte, and cathode thickness are 1 mm, ∼12 μm, and ∼11 μm, respectively. The porous anode support, $BaCe_{0.2}Zr_{0.7}Y_{0.1}O_{3-\delta}$ (BCZY27)−Ni, reveals a homogeneous and defect-free microstructure with a pore size of several microns, as shown in Figure 2a,b. This microstructure facilitates gas diffusion in the anode and has good mechanical strength. The as-printed BCZY27 electrolyte is uniform and dense without visible pinholes or cracks. It adheres well to the porous electrodes with no delamination, as shown in Figure 2c. Figure 2d shows a uniform cathode, $BaCo_{0.4}Fe_{0.4}Zr_{0.1}Y_{0.1}O_{3-\delta}$ (BCFZY0.1), with fine porosity and nanosized grains, contributing to rapid gas transport and lots of triple-phase boundary sites, thus leading to an excellent electrochemical performance. X-ray diffraction measurements verified the electrolyte's and electrodes' phase structures (Figure S5). Therefore, the as-expected phase structures, compositions, and microstructures can be accurately controlled by the 3DP.

The as-fabricated single tubular PCFCs demonstrate encouraging electrochemical performances under a hydrogen/air gradient from 650 to 400 °C. We first took an example of a single tubular PCFC with an effective area of 3.0 cm^2. Figure 3a shows the corresponding current−voltage (I−V) curves. The tubular cell's open-circuit voltages (OCVs) were 1.028, 1.072, 1.105, and 1.135 V at 650, 600, 550, and 500 °C, respectively. These OCVs are close to the theoretical values, indicating that electronic leakage in the electrolyte is negligible and that the printed electrolyte is free of cracks and pinholes, achieving high gas tightness. The single tubular cell yielded maximum power densities (MPDs) of 375, 281, 218, and 164 mW cm^{-2} at 650, 600, 550, and 500 °C, respectively. These MPDs are comparable with reported results on tubular PCFCs fabricated by the conventional methods, for example, extrusion (312 mW cm^{-2} with an effective area of 2.07 cm^2 at 600 °C),[15] slip casting (170 mW cm^{-2} with an effective area of 1.79 cm^2 at 600 °C),[11] and phase inversion (260 mW cm^{-2} with an effective area of 0.65 cm^2 at 600 °C)[24] methods. Although some single tubular cells showed slightly higher MPDs, their effective areas were below 2.5 cm^2. This tubular PCFC, however, needs to be further optimized (electrode and electrolyte materials) before it can compete with these systems.

To assess the impact of resistance on the power densities, electrochemical impedance spectroscopy (EIS) measurement was performed under OCV conditions at 400−650 °C. The ohmic resistance can be obtained from the high-frequency intersection of the EIS arc on the real axis, which is related to charge conductions in the electrolyte and the contact between the electrolyte and electrodes; in contrast, the polarization resistance determined from the width of the intersects on the real axis is associated with the electrode reactions. The area-specific polarization resistances (ASR_p) and ohmic resistances (ASR_o) at 400−650 °C were obtained from the fitting of the EIS curves (Figures 3b and S6a) by Zview software. The ohmic resistance decreases from 1.09 to 0.56 Ω cm^2, while the polarization resistance reduces from 0.15 to 0.05 Ω cm^2 when increasing the temperature from 550 to 650 °C. They were then presented as Arrhenius plots in Figure 3c. The activation energy of ASR_p and ASR_o is ∼0.95 and ∼0.30 eV, respectively, consistent with previously reported results[1,43] on similar electrolytes and electrodes. To gain further understanding of the reaction mechanism, the distribution of the relaxation time (DRT) technique was utilized to deconvolute the impedance response (Figure S6c). The DRT plot can be separated into three distinct frequency sections: high frequency (>10^4 Hz), intermediate frequency (10−10^4 Hz), and low frequency (10^{-2}−10 Hz), which is consistent with the reports on PCFCs.[44,45] The high-, intermediate-, and low-frequency peaks correspond to the ion transfer across the electrolyte/electrode interface, surface exchange or ion transfer at the electrode bulk, and mass transfer in the electrode, respectively. Table S1 summarized the ASRs of tubular PCFCs fabricated by different methods at 650 °C. The ASR_p of our 3D-printed tubular PCFC is far smaller than many reports on tubular PCFCs, even those achieving very high MPDs via phase inversion methods (0.11 Ω cm^2 at 650 °C).[46] The low ASR_p is attributed to the uniform porous microstructure of the electrodes and the nanoscale grain size in the BCFZY0.1 cathode thin film, which could facilitate the gas diffusion in the electrodes and remarkably expand TPB sites for the cathode reaction. Generally, the tubular cell shows high ohmic losses due to the geometrical configuration of the current collectors, which reduces the overall performance.[47] For the as-fabricated single tubular PCFCs, the ASR_o values (0.56 Ω cm^2 at 650 °C for the 3.0 cm^2 tube, 0.63 Ω cm^2 at 650 °C for the 12.5 cm^2 tube) are comparable with those prepared by conventional methods (e.g., 0.94 Ω cm^2 at 650 °C for a 2.07 cm^2 tube via extrusion;[15] 0.59 Ω cm^2 at 650 °C for a 1.6 cm^2 tube via slip casting;[22] 0.27 Ω cm^2 at 650 °C for a 1 cm^2 tube via phase inversion,[29] as shown in Table S1), although we used BCZY27 as the electrolyte. Generally, BCZY27 possesses much lower conductivity (∼21 mS/cm under wet oxygen at 650 °C)[48] than $BaCe_{0.7}Zr_{0.1}Y_{0.1}Yb_{0.1}O_{3-\delta}$ (BCZYYb) (∼38 to 70 mS/cm under wet oxygen at 650 °C).[49,50] However, BCZY27 has far better chemical stability against CO_2 and steam-rich environments. These results again highlight the excellent manufacturing ability of the 3DP technique in producing tubular PCFCs. On the other hand, the power densities of the 3D-printed tubular PCFCs could be further enhanced by utilizing electrolyte materials with higher ionic conductivities to alleviate the dominating ohmic losses.

In addition to the high ohmic losses deteriorating the overall electrocatalytic performances, the large cell size would introduce many other challenges, such as difficulty in achieving homogeneous microstructures, the elongated path of the current collection, and higher risk of exhibiting cracks/delamination. Due to these effects, relatively small-sized (<2.5 cm^2) tubular PCFCs fabricated via conventional methods are often reported. In sharp contrast, this work demonstrates promising power output in large-scale single cells with an effective area of up to 12.5 cm^2. As shown in Figure 3d, the single tubular PCFC with an effective area of 12.5 cm^2 can achieve a power output as high as 2.45 W at 650 °C, the highest reported value among its counterparts in Table S2. In addition, much higher power densities (∼197 mW cm^{-2} at 650 °C, as shown in Figure S7) were achieved, compared with the tubular PCFCs (∼78 mW cm^{-2} with an effective area of 7.5

https://doi.org/10.1021/acsenergylett.3c01345
ACS Energy Lett. 2023, 8, 3545−3551

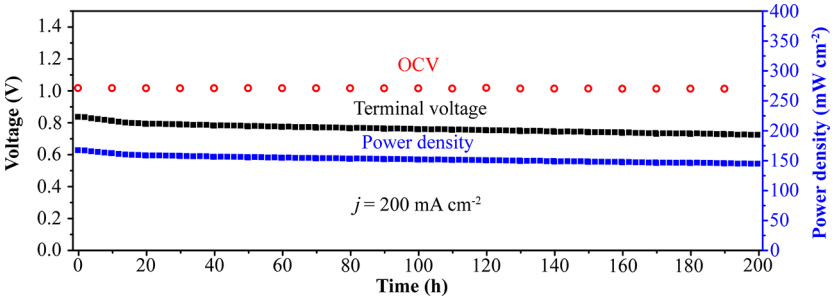

Figure 4. Long-term stability of the tubular PCFC with a constant current density of 200 mA cm^{-2} at 650 °C.

cm^2 at 700 °C)[14] obtained via an extrusion method using the same BCZY27 electrolyte material. These results imply that our 3DP-printed single cells are uniform, mechanically robust, and highly scalable, all of which are difficult to realize by conventional methods.

To assess the long-term stability of the manufactured tubular PCFCs, we tested the single cell under a current of 200 mA cm^{-2} for 200 h at 650 °C, as shown in Figure 4. During the first 15 h of operation, the power density and cell terminal voltage slightly dropped (~4.3%), which could be ascribed to the initial stabilization of the cell at 650 °C. After that, the cell showed a negligible degradation rate of 0.00039 V h^{-1} for the rest of the test duration. The tiny degradation may be associated with the current collector peeling during long-term operation. This is evidenced by an increasing dominating ohmic resistance and a comparatively stable polarization resistance (Figure S8), consistent with the reported work on tubular PCFCs.[18] In addition, the cell maintained a desirable microstructure after the long-term test (Figure S9). The anode−electrolyte and electrolyte−cathode interfaces have no delamination or cracks. Moreover, the electrolyte exhibits excellent uniformity and is intact without any pinholes or cracks. The cathode thin film maintains the homogeneous nanoscale microstructure. These results demonstrate that printed tubular PCFCs show good long-term stability and are promising for practical applications.

In summary, we reported a facile and cost-effective 3DP technique for manufacturing scalable tubular PCFCs. The as-fabricated single tubular PCFC showed a well-controlled microstructure consisting of tubular BCZY27−NiO anode support, dense BCZY27 electrolyte thin film, and porous BCFZY0.1 cathode thin film. Although they possess larger active areas, their exhibited area-specific resistances are comparable to those of tubular PCFCs fabricated via state-of-the-art conventional methods. A high total power of 2.45 W was achieved in a large-scale (~12.5 cm^2) single cell at 650 °C under a hydrogen/air gradient. This study suggested that the 3DP technique can manufacture PCFCs with high-power output and long life spans, ushering in new possibilities for commercializing scalable tubular PCFCs.

■ ASSOCIATED CONTENT

Supporting Information

The Supporting Information is available free of charge at https://pubs.acs.org/doi/10.1021/acsenergylett.3c01345.

Experimental details and supplementary figures, including 3D printing system, fuel cell testing setup, crystallization phase structure, cell microstructure, and electrochemical performance (PDF)

■ AUTHOR INFORMATION

Corresponding Authors

Jiawei Zhang − *Department of Materials Science and Engineering, Clemson University, Clemson, South Carolina 29634, United States;* orcid.org/0000-0001-9635-154X; Email: jiawei4@clemson.edu

Jianhua Tong − *Department of Materials Science and Engineering, Clemson University, Clemson, South Carolina 29634, United States;* orcid.org/0000-0002-0684-1658; Email: jianhut@clemson.edu

Authors

Minda Zou − *Department of Materials Science and Engineering, Clemson University, Clemson, South Carolina 29634, United States*

Jacob Conrad − *Department of Materials Science and Engineering, Clemson University, Clemson, South Carolina 29634, United States*

Bridget Sheridan − *Department of Materials Science and Engineering, Clemson University, Clemson, South Carolina 29634, United States*

Hua Huang − *Department of Materials Science and Engineering, Clemson University, Clemson, South Carolina 29634, United States*

Shenglong Mu − *Department of Materials Science and Engineering, Clemson University, Clemson, South Carolina 29634, United States*

Tianyi Zhou − *Department of Materials Science and Engineering, Clemson University, Clemson, South Carolina 29634, United States*

Zeyu Zhao − *Department of Materials Science and Engineering, Clemson University, Clemson, South Carolina 29634, United States*

Kyle S. Brinkman − *Department of Materials Science and Engineering, Clemson University, Clemson, South Carolina 29634, United States;* orcid.org/0000-0002-2219-1253

Hai Xiao − *Department of Electrical and Computer Engineering, Clemson University, Clemson, South Carolina 29634, United States*

Fei Peng − *Department of Materials Science and Engineering, Clemson University, Clemson, South Carolina 29634, United States;* orcid.org/0000-0002-3924-9028

Complete contact information is available at: https://pubs.acs.org/10.1021/acsenergylett.3c01345

Author Contributions

M. Z., J. Z., and J. T. conceived of the experimental study and wrote the manuscript. M. Z. and J. Z. executed the experiments and did the data analysis. J. C., B. S., H. H., S. M., T. Z., and Z. Z. assisted in the preparation of the precursor powders, pastes,

https://doi.org/10.1021/acsenergylett.3c01345
ACS Energy Lett. 2023, 8, 3545−3551

and thin film coating. K. S. B., H. X., and F. P. provided technical support and scientific discussion. All authors discussed the results and commented on the manuscript.

Notes

The authors declare no competing financial interest.

■ ACKNOWLEDGMENTS

This material is based upon work supported by the US Department of Energy's Office of Fossil Energy and Carbon Management (FECM) Award Number DE-FE0031871. This work was partly supported by the National Aeronautics and Space Administration (NASA) under Grant #80NSSC20M0233 (NASA).

■ REFERENCES

(1) Duan, C.; Tong, J.; Shang, M.; Nikodemski, S.; Sanders, M.; Ricote, S.; Almansoori, A.; O'Hayre, R. Readily Processed Protonic Ceramic Fuel Cells with High Performance at Low Temperatures. *Science* **2015**, *349* (6254), 1321−1326.

(2) Duan, C.; Kee, R. J.; Zhu, H.; Karakaya, C.; Chen, Y.; Ricote, S.; Jarry, A.; Crumlin, E. J.; Hook, D.; Braun, R.; Sullivan, N. P.; O'Hayre, R. Highly Durable, Coking and Sulfur Tolerant, Fuel−flexible Protonic Ceramic Fuel Cells. *Nature* **2018**, *557* (7704), 217−222.

(3) Cao, J.; Ji, Y.; Shao, Z. Perovskites for Protonic Ceramic Fuel Cells: A Review. *Energy Environ. Sci.* **2022**, *15*, 2200−2232.

(4) Bello, I. T.; Zhai, S.; He, Q.; Cheng, C.; Dai, Y.; Chen, B.; Zhang, Y.; Ni, M. Materials Development and Prospective for Protonic Ceramic Fuel Cells. *Int. J. Energy Res.* **2022**, *46* (3), 2212−2240.

(5) Weil, K. S.; Koeppel, B. J. Thermal Stress Analysis of the Planar SOFC Bonded Compliant Seal Design. *Int. J. Hydrogen Energy* **2008**, *33* (14), 3976−3990.

(6) Lin, C. K.; Chen, T. T.; Chyou, Y. P.; Chiang, L. K. Thermal Stress Analysis of a Planar SOFC Stack. *J. Power Sources* **2007**, *164* (1), 238−251.

(7) Qi, X.; Akin, F. T.; Lin, Y. S. Ceramic−Glass Composite High Temperature Seals for Dense Ionic−conducting Ceramic Membranes. *J. Membr. Sci.* **2001**, *193* (2), 185−193.

(8) Di Felice, L.; Middelkoop, V.; Anzoletti, V.; Snijkers, F.; van Sint Annaland, M.; Gallucci, F. New High Temperature Sealing Technique and Permeability Data for Hollow Fiber BSCF Perovskite Membranes. *Chem. Eng. Process.* **2016**, *107*, 206−219.

(9) Zhu, L.; O'Hayre, R.; Sullivan, N. P. High Performance Tubular Protonic Ceramic Fuel Cells via Highly−scalable Extrusion Process. *Int. J. Hydrogen Energy* **2021**, *46* (54), 27784−27792.

(10) Wang, Z.; Chen, T.; Dewangan, N.; Li, Z.; Das, S.; Pati, S.; Li, Z.; Lin, J. Y. S.; Kawi, S. Catalytic Mixed Conducting Ceramic Membrane Reactors for Methane Conversion. *React. Chem. Eng.* **2020**, *5* (10), 1868−1891.

(11) Amiri, T.; Singh, K.; Sandhu, N. K.; Hanifi, A. R.; Etsell, T. H.; Luo, J.−L.; Thangadurai, V.; Sarkar, P. High Performance Tubular Solid Oxide Fuel Cell Based on $Ba_{0.5}Sr_{0.5}Ce_{0.6}Zr_{0.2}Gd_{0.1}Y_{0.1}O_{3-\delta}$ Proton Conducting Electrolyte. *J. Electrochem. Soc.* **2018**, *165* (10), F764.

(12) Panthi, D.; Hedayat, N.; Woodson, T.; Emley, B. J.; Du, Y. Tubular Solid Oxide Fuel Cells Fabricated by a Novel Freeze Casting Method. *J. Am. Ceram. Soc.* **2020**, *103* (2), 878−888.

(13) Chen, C.; Dong, Y.; Li, L.; Wang, Z.; Liu, M.; Rainwater, B. H.; Bai, Y. High Performance of Anode Supported $BaZr_{0.1}Ce_{0.7}Y_{0.1}Yb_{0.1}O_{3-\delta}$ Proton−conducting Electrolyte Micro−tubular Cells with Asymmetric Structure for IT−SOFCs. *J. Electroanal. Chem.* **2019**, *844*, 49−57.

(14) Robinson, S.; Manerbino, A.; Grover Coors, W.; Sullivan, N. P. Fabrication and Performance of Tubular, Electrode−supported $BaCe_{0.2}Zr_{0.7}Y_{0.1}O_{3-\delta}$ Fuel Cells. *Fuel Cells* **2013**, *13* (4), 584−591.

(15) Min, S. H.; Song, R. H.; Lee, J. G.; Park, M. G.; Ryu, K. H.; Jeon, Y. K.; Shul, Y. G. Fabrication of Anode−supported Tubular $Ba(Zr_{0.1}Ce_{0.7}Y_{0.2})O_{3-\delta}$ Cell for Intermediate Temperature Solid Oxide Fuel Cells. *Ceram. Int.* **2014**, *40* (1), 1513−1518.

(16) Yamaguchi, T.; Shimada, H.; Honda, U.; Kishimoto, H.; Ishiyama, T.; Hamamoto, K.; Sumi, H.; Suzuki, T.; Fujishiro, Y. Development of Anode−supported Electrochemical Cell Based on Proton−conductive $Ba(Ce,Zr)O_3$ Electrolyte. *Solid State Ion* **2016**, *288*, 347−350.

(17) Nowicki, K. M.; Carins, G.; Bayne, J.; Tupberg, C.; Irvine, G. J.; Irvine, J. T. S. Characterisation of Direct Ammonia Proton Conducting Tubular Ceramic Fuel Cells for Maritime Applications. *J. Mater. Chem. A* **2022**, *11* (1), 352−363.

(18) Cao, D.; Zhou, M.; Yan, X.; Liu, Z.; Liu, J. High Performance Low−temperature Tubular Protonic Ceramic Fuel Cells Based on Barium Cerate−zirconate Electrolyte. *Electrochem. Commun.* **2021**, *125*, 106986.

(19) Chen, C.; Liu, M.; Bai, Y.; Yang, L.; Xie, E.; Liu, M. Anode−supported Tubular SOFCs Based on $BaZr_{0.1}Ce_{0.7}Y_{0.1}Yb_{0.1}O_{3-\delta}$ Electrolyte Fabricated by Dip Coating. *Electrochem. Commun.* **2011**, *13* (6), 615−618.

(20) Beyribey, B.; Bayne, J.; Persky, J. The Effect of Dip−coating Parameters on the Thickness and Uniformity of BCZYZ Electrolyte Layer on Porous NiO−BCZYZ Tubular Supports. *Ceram. Int.* **2022**, *48* (5), 6046−6051.

(21) Hanifi, A. R.; Sandhu, N. K.; Etsell, T. H.; Luo, J. L.; Sarkar, P. Fabrication and Characterization of a Tubular Ceramic Fuel Cell Based on $BaZr_{0.1}Ce_{0.7}Y_{0.1}Yb_{0.1}O_{3-\delta}$ Proton Conducting Electrolyte. *J. Power Sources* **2017**, *341*, 264−269.

(22) Vafaeenezhad, S.; Sandhu, N. K.; Hanifi, A. R.; Etsell, T. H.; Sarkar, P. Development of Proton Conducting Fuel Cells Using Nickel Metal Support. *J. Power Sources* **2019**, *435*, 226763.

(23) Ricote, S.; Kee, R. J.; Coors, W. G. Slip Casting and Solid−state Reactive Sintering of BCZY($BaCe_xZr_{0.9-x}Y_{0.1}O_{3-d}$)−NiO/BCZY Half−cells. *Membranes* **2022**, *12* (2), 242.

(24) Zhao, F.; Jin, C.; Yang, C.; Wang, S.; Chen, F. Fabrication and Characterization of Anode−supported Micro−tubular Solid Oxide Fuel Cell Based on $BaZr_{0.1}Ce_{0.7}Y_{0.1}Yb_{0.1}O_{3-\delta}$ Electrolyte. *J. Power Sources* **2011**, *196* (2), 688−691.

(25) Zhao, L.; Zhang, X.; He, B.; Liu, B.; Xia, C. Micro−tubular Solid Oxide Fuel Cells with Graded Anodes Fabricated with a Phase Inversion Method. *J. Power Sources* **2011**, *196* (3), 962−967.

(26) He, B.; Ding, D.; Ling, Y.; Zhao, L.; Cheng, J. Fabrication and Evaluation of Stable Micro Tubular Solid Oxide Fuel Cells with BZCY−BZY Bi−layer Proton Conducting Electrolytes. *Int. J. Hydrogen Energy* **2014**, *39* (33), 19087−19092.

(27) Ren, C.; Wang, S.; Liu, T.; Lin, Y.; Chen, F. Fabrication of Micro−Tubular Solid Oxide Fuel Cells Using Sulfur−free Polymer Binder via a Phase Inversion Method. *J. Power Sources* **2015**, *290*, 1−7.

(28) Chen, C.; Dong, Y.; Li, L.; Wang, Z.; Liu, M.; Rainwater, B. H.; Bai, Y. Electrochemical Properties of Micro−tubular Intermediate Temperature Solid Oxide Fuel Cell with Novel Asymmetric Structure Based on $BaZr_{0.1}Ce_{0.7}Y_{0.1}Yb_{0.1}O_{3-\delta}$ Proton Conducting Electrolyte. *Int. J. Hydrogen Energy* **2019**, *44* (31), 16887−16897.

(29) Dong, Y.; Chen, C.; Liu, M.; Rainwater, B. H.; Bai, Y. Enhancement of Electrochemical Properties, Impedance and Resistances of Micro−tubular IT−SOFCs with Novel Asymmetric Structure Based on $BaZr_{0.1}Ce_{0.7}Y_{0.1}Yb_{0.1}O_{3-\delta}$ Proton Conducting Electrolyte. *Fuel Cells* **2020**, *20* (1), 70−79.

(30) Mat, A.; Canavar, M.; Timurkutluk, B.; Kaplan, Y. Investigation of Micro−tube Solid Oxide Fuel Cell Fabrication Using Extrusion Method. *Int. J. Hydrogen Energy* **2016**, *41* (23), 10037−10043.

(31) Sukeshini, M. A.; Cummins, R.; Reitz, T. L.; Miller, R. M. Ink−Jet Printing: A Versatile Method for Multilayer Solid Oxide Fuel Cells Fabrication. *J. Am. Ceram. Soc.* **2009**, *92* (12), 2913−2919.

(32) Han, G. D.; Bae, K.; Kang, E. H.; Choi, H. J.; Shim, J. H. Inkjet Printing for Manufacturing Solid Oxide Fuel Cells. *ACS Energy Lett.* **2020**, *5* (5), 1586−1592.

(33) Park, J. S.; Choi, H. J.; Han, G. D.; Koo, J.; Kang, E. H.; Kim, D. H.; Bae, K.; Shim, J. H. High−performance Protonic Ceramic Fuel

https://doi.org/10.1021/acsenergylett.3c01345
ACS Energy Lett. 2023, 8, 3545−3551

Cells with a $PrBa_{0.5}Sr_{0.5}Co_{1.5}Fe_{0.5}O_{5+\delta}$ Cathode with Palladium−rich Interface Coating. *J. Power Sources* **2021**, *482*, 229043.
(34) Sukeshini A., M.; Meisenkothen, F.; Gardner, P.; Reitz, T. L. Aerosol Jet® Printing of Functionally Graded SOFC Anode Interlayer and Microstructural Investigation by Low Voltage Scanning Electron Microscopy. *J. Power Sources* **2013**, *224*, 295−303.
(35) Sukeshini, A. M.; Gardner, P.; Meisenkothen, F.; Jenkins, T.; Miller, R.; Rottmayer, M.; Reitz, T. L. Aerosol Jet Printing and Microstructure of SOFC Electrolyte and Cathode Layers. *ECS Trans* **2011**, *35* (1), 2151.
(36) Wei, L.; Zhang, J.; Yu, F.; Zhang, W.; Meng, X.; Yang, N.; Liu, S. A Novel Fabrication of Yttria−stabilized−zirconia Dense Electrolyte for Solid Oxide Fuel Cells by 3D Printing Technique. *Int. J. Hydrogen Energy* **2019**, *44* (12), 6182−6191.
(37) Pesce, A.; Hornés, A.; Núñez, M.; Morata, A.; Torrell, M.; Tarancón, A. 3D Printing the Next Generation of Enhanced Solid Oxide Fuel and Electrolysis Cells. *J. Mater. Chem. A* **2020**, *8* (33), 16926−16932.
(38) Zhang, J.; Wei, L.; Meng, X.; Yu, F.; Yang, N.; Liu, S. Digital Light Processing−stereolithography Three−dimensional Printing of Yttria−stabilized Zirconia. *Ceram. Int.* **2020**, *46* (7), 8745−8753.
(39) Miyamoto, K.; Koga, H.; Izumi, M.; Mizui, M.; Nishiguchi, H. Study on Fabrication of Anodes for SOFCs with 3D Printing Technology. *ECS Trans* **2020**, *96* (1), 219.
(40) Manogharan, G.; Kioko, M.; Linkous, C. Binder Jetting: A Novel Solid Oxide Fuel−cell Fabrication Process and Evaluation. *JOM* **2015**, *67*, 660−667.
(41) Berges, C.; Wain, A.; Andújar, R.; Naranjo, J. A.; Gallego, A.; Nieto, E.; Herranz, G.; Campana, R. Fused Filament Fabrication for Anode Supported SOFC Development: Towards Advanced, Scalable and Cost−competitive Energetic Systems. *Int. J. Hydrogen Energy* **2021**, *46* (51), 26174−26184.
(42) Huang, W.; Finnerty, C.; Sharp, R.; Wang, K.; Balili, B. High-performance 3D Printed Microtubular Solid Oxide Fuel Cells. *Adv. Mater. Technol.* **2017**, *2* (4), 1600258.
(43) An, H.; Lee, H. W.; Kim, B. K.; Son, J. W.; Yoon, K. J.; Kim, H.; Shin, D.; Ji, H.− I.; Lee, J. H. A 5 × 5 cm^2 Protonic Ceramic Fuel Cell with a Power Density of 1.3 W cm^{-2} at 600 °C. *Nat. Energy* **2018**, *3* (10), 870−875.
(44) Ren, R.; Yu, X.; Wang, Z.; Xu, C.; Song, T.; Sun, W.; Qiao, J.; Sun, K. Fluorination Inductive Effect Enables Rapid Bulk Proton Diffusion in $BaCo_{0.4}Fe_{0.4}Zr_{0.1}Y_{0.1}O_{3-\delta}$ Perovskite Oxide for High−activity Protonic Ceramic Fuel Cell Cathode. *Appl. Catal., B* **2022**, *317*, 121759.
(45) Bello, I. T.; Yu, N.; Song, Y.; Wang, J.; Chan, T. S.; Zhao, S.; Li, Z.; Dai, Y.; Yu, J.; Ni, M. Electrokinetic Insights into the Triple Ionic and Electronic Conductivity of a Novel Nanocomposite Functional Material for Protonic Ceramic Fuel Cells. *Small* **2022**, *18* (40), 2203207.
(46) Pan, Y.; Zhang, H.; Xu, K.; Zhou, Y.; Zhao, B.; Yuan, W.; Sasaki, K.; Choi, Y. M.; Chen, Y.; Liu, M. A High−performance and Durable Direct NH_3 Tubular Protonic Ceramic Fuel Cell Integrated with an Internal Catalyst Layer. *Appl. Catal., B* **2022**, *306*, 121071.
(47) Sammes, N. M.; Du, Y.; Bove, R. Design and Fabrication of a 100 W Anode Supported Micro−tubular SOFC Stack. *J. Power Sources* **2005**, *145* (2), 428−434.
(48) Heras-Juaristi, G.; Pérez-Coll, D.; Mather, G. C. Temperature Dependence of Partial Conductivities of the $BaZr_{0.7}Ce_{0.2}Y_{0.1}O_{3-\delta}$ Proton Conductor. *J. Power Sources* **2017**, *364*, 52−60.
(49) Yang, L.; Wang, S.; Blinn, K.; Liu, M.; Liu, Z.; Cheng, Z.; Liu, M. Enhanced Sulfur and Coking Tolerance of a Mixed Ion Conductor for SOFCs: $BaZr_{0.1}Ce_{0.7}Y_{0.2-x}Yb_xO_{3-\delta}$. *Science* **2009**, *326* (5949), 126−129.
(50) Zhou, X.; Liu, L.; Zhen, J.; Zhu, S.; Li, B.; Sun, K.; Wang, P. Ionic Conductivity, Sintering and Thermal Expansion Behaviors of Mixed Ion Conductor $BaZr_{0.1}Ce_{0.7}Y_{0.1}Yb_{0.1}O_{3-\delta}$ Prepared by Ethylene Diamine Tetraacetic Acid Assisted Glycine Nitrate Process. *J. Power Sources* **2011**, *196* (11), 5000−5006.

https://doi.org/10.1021/acsenergylett.3c01345
ACS Energy Lett. 2023, 8, 3545−3551